Dynamics of the excitations of a quantum dot in a microcavity

J. I. Perea, D. Porras,* and C. Tejedor
Departamento de Física Teórica de la Materia Condensada, Universidad Autónoma de Madrid, 28049 Madrid, Spain
(Received 21 October 2003; revised manuscript received 15 June 2004; published 9 September 2004)

We study the dynamics of a quantum dot embedded in a three-dimensional microcavity in the strong coupling regime in which the quantum dot exciton has an energy close to the frequency of a confined cavity mode. Under the continuous pumping of the system, the confined electron and hole can recombine either by spontaneous emission through a leaky mode or by stimulated emission of a cavity mode that can escape from the cavity. The numerical integration of a master equation including all these effects gives the dynamics of the density matrix. By using the quantum regression theorem, we compute the first- and second-order coherence functions required to calculate the photon statistics and the spectrum of the emitted light. Our main result is the determination of a range of parameters in which a state of cavity modes with Poissonian or sub-Poissonian (nonclassical) statistics can be built up within the microcavity. Depending on the relative values of pumping and rate of stimulated emission, either one or two peaks close to the excitation energy of the dot and/or to the natural frequency of the cavity are observed in the emission spectrum. The physics behind these results is discussed.

DOI: 10.1103/PhysRevB.70.115304 PACS number(s): 78.67.Hc, 42.50.Ct

I. INTRODUCTION

Quantum electrodynamics of atoms within optical cavities is a well-understood problem that has produced many results of both fundamental and practical interest.[1–4] The current capability of using semiconductors technology to grow quantum dots (QD) embedded in microcavities seems very promising to reproduce and control the properties in a solid-state system that could be integrated in electronic or optical devices. The essential physics of such a system is the coupling between the QD excitations and the photonic cavity modes as well as the possibility of interaction with the external world through the pumping of the system and the subsequent emission of light. The main goal is the control of the emitted light and its quantum properties. Therefore it is possible to build up high-efficiency light-emitting diodes, low-threshold lasers, and single-photon sources.

We concentrate here on a problem, not far from the actual situation in several experiments[5–11] in which a single QD is embedded in either a pillar, a disk, or a photonic crystal microcavity confining photons in the three spatial directions. The system is pumped either by electrically injecting electrons and holes that tunnel into the QD[6] or by pumping excitons in the QD.[5,7,9–11] Light emission from the system takes place both by cavity mode decay and by spontaneous emission of leaky modes. All these pumping and emission mechanisms introduce decoherence affecting the quantum properties of the system.

The lowest energy excitation of a neutral QD is an electron-hole pair, usually labeled as exciton. Due to the fermionic character of its components, this exciton state can only be singly occupied having a degeneracy related to the possible values of the third component of the total angular momentum. This quantum number is usually referred to as the spin of the exciton. Among all these states, only two cases—those corresponding to ±1—are of interest in our problem due to their possible coupling with photons. The next excitation corresponds to the case in which both +1 and −1 excitons are occupied. This biexciton state has an energy different to twice that of a single exciton due to the Coulomb interaction of their components. This spectrum presents interesting alternatives,[12] which we intend to study in future work, while here we restrict to simplest case in which we consider only excitons with a given spin. This assumption is well justified in the case of experiments in which the system would be pumped with polarized light, so that excitons with a given angular momentum would be created in the system.[13] We also assume that spin-flip mechanisms are slow as compared with typical time scales in our system. Other single-particle states of the QD, above the exciton energy, can be neglected because they are not strongly coupled to the cavity mode in the case of resonance or quasiresonance between the exciton and the confined photon. Under these conditions, the problem reduces to that of a two-level artificial atom embedded in the optical cavity. We are going to show that, in spite of this simplification, the system presents a very rich variety of physical situations.

The problem of a two-level system coupled to a single cavity mode under different conditions and approximations has received a lot of attention, mainly in the field of quantum optics.[1–4,14,15] Of particular interest is the study of the possible sub-Poissonian radiation when cavity losses and pumping dominate onto the spontaneous emission of leaky modes. The aim of our work is an exhaustive analysis of the different regimes of parameters to determine the role played by the different physical mechanisms in the quantum properties of both the internal state of the system and the light emitted in the steady regime under continuous incoherent pumping. Since the case of perfect resonance has been already studied,[15] we will make emphasis on the effects appearing in the more realistic situation of having a finite detuning between the QD exciton and the cavity photon.

The paper is organized as follows: In Sec. II we describe the model Hamiltonian and master equation that allows to calculate the evolution of the populations and coherences of the energy levels. By means of the quantum regression theo-

rem, we can use our master equation to calculate cavity photon statistics and the spectrum of the emitted light. In Sec. III we present the results for the time evolution of the magnitudes of interest in different ranges of parameters characterizing different physical situations. The spectrum of the light emitted by the system is presented and discussed in Sec. IV. Section V is devoted to a summary of the work.

II. THEORETICAL FRAMEWORK

We consider a single QD inside a semiconductor microcavity that is continuously and incoherently pumped. Our system is initially in its ground state and evolves until it reaches the steady state. In order to describe the time evolution of the QD-cavity system we use a master equation that includes the strong exciton-photon coupling, the nonresonant pump, and the interaction with the environment that is responsible for dissipation.

A. The Hamiltonian

The physics of a QD strongly coupled with a single cavity mode is described by the Hamiltonian

$$H = H_S + H_{RS} + H_R. \tag{1}$$

H_S and H_R are the Hamiltonian for the QD-cavity system, and the environment (reservoirs), respectively. The term H_{RS} describes the interaction between the QD-cavity system and the reservoirs. H_S is given by the usual Jaynes-Cummings Hamiltonian,[2,4] which describes the interaction of a two-level system with a single mode of the electromagnetic field,

$$H_S = H_0 + H_{X-C},$$

$$H_0 = \omega_X |X\rangle\langle X| + (\omega_X - \Delta) a^\dagger a,$$

$$H_{X-C} = g(\sigma a^\dagger + a\sigma^\dagger). \tag{2}$$

We have introduced ladder operators $\sigma^\dagger = |X\rangle\langle G|$, $\sigma = |G\rangle\langle X|$ connecting the ground $|G\rangle$ and excited (exciton) $|X\rangle$ states of the QD with energies zero and ω_X, respectively (we take $\hbar = 1$). $a^\dagger$ creates a cavity photon with energy $(\omega_X - \Delta)$. The coupling term H_{X-C} in Eq. (2) describes the exciton-photon coupling in the Rotating Wave Approximation.[1–3]

H_{RS} contains the coupling to external reservoirs including the following three processes:

(i) The continuous and incoherent pumping of the QD by annihilating $(c_{R'})$ an electron-hole pair from an external reservoir R' (representing either electrical injection or the capture of excitons optically created at frequencies larger than the typical ones of our system) and creation $(d^\dagger_{R''})$ a phonon emitted to a reservoir R'' in order to take care of energy conservation

$$\sum_{R',R''} \mu_{R',R''} [d^\dagger_{R''} c_{R'} \sigma^\dagger + \sigma c^\dagger_{R'} d_{R''}], \tag{3}$$

(ii) The direct coupling of the QD exciton to the leaky modes, that is, to the photonic modes, with energy different from the cavity mode, that have a residual density of states inside the microcavity. This process is responsible for the dissipation of the excitonic degrees of freedom by the spontaneous emission to an external reservoir R of photons created by $b^\dagger_R$

$$\sum_R \lambda_{lR} [\sigma b^\dagger_R + b_R \sigma^\dagger], \tag{4}$$

(iii) The escape of the cavity mode out of the microcavity due to the incomplete reflectance of the mirrors. The cavity mode is thus coupled to the continuum of photonic modes out of the microcavity. This process produces the direct dissipation of the cavity mode

$$H_{CE} = \sum_R \lambda_R (a b^\dagger_R + b_R a^\dagger). \tag{5}$$

The last term in Eq. (1), H_R, describes the external reservoirs of harmonic oscillators (photons, phonons, electron-hole pairs, …), not being necessary to detail them explicitly. The three terms H_{RS} have coupling constants $\mu_{R',R''}$, λ_R, and λ_{lR}, which depend on the particular mode (R, R', or R'') of each external reservoir. The operators a, b_R, $c_{R'}$, and $d_{R''}$ have bosonic commutation rules as they correspond to harmonic oscillators. Since we are interested in the strong coupling regime, the first three terms, H_0 and H_{X-C} are treated exactly. That means that one could work in the framework usually known as the "dressed atom picture." However, in order to clarify the different pumping and losses mechanisms, it is preferable to work in basis $(|Gn\rangle; |Xn\rangle)$ in terms of the number of cavity photons n and bare ground G and exciton X states of the QD.

B. Master equation

We have made the whole algebra for a general case in which reservoirs are at finite temperature. However, the main physics already occurs for zero temperature, which is the case we present hereafter in this paper.

We define the reduced density matrix, ρ, for the exciton-photon system by tracing out the reservoir degrees of freedom in the total density matrix ρ_T

$$\rho = Tr_R(\rho_T). \tag{6}$$

In the interaction picture with respect to $H_{X-C} + H_{RS}$ in Eqs. (1) and (2), ρ satisfies the master equation[2,3]

$$\frac{d}{dt}\rho = \frac{i}{\hbar}[\rho, H_S] + \frac{\kappa}{2}(2a\rho a^\dagger - a^\dagger a\rho - \rho a^\dagger a) + \frac{\gamma}{2}(2\sigma\rho\sigma^\dagger - \sigma^\dagger\sigma\rho - \rho\sigma^\dagger\sigma) + \frac{P}{2}(2\sigma^\dagger\rho\sigma - \sigma\sigma^\dagger\rho - \rho\sigma\sigma^\dagger). \tag{7}$$

The master equation is obtained under the usual Born-Markov approximation for the interaction H_{RS} between the QD-cavity system and the reservoirs, but the strong exciton-cavity photon coupling H_{X-C} is described exactly. κ is the decay of the cavity photon by escaping through the microcavity mirrors, γ is the decay of the QD exciton by the spontaneous emission into leaky modes, and P is the rate of continuous incoherent pumping of the QD exciton. By means of

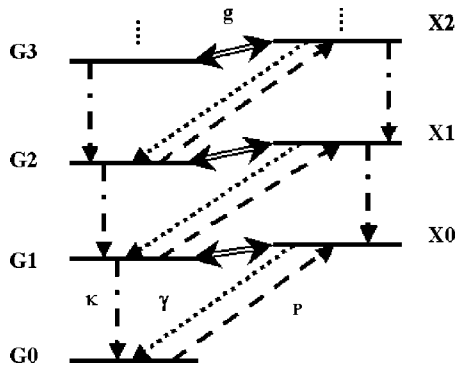

FIG. 1. Ladder of levels (continuous lines) for a two-state QD coupled to a single optical mode of a microcavity. States labeled as Gn with $n=0,1,2,\ldots$ correspond to having the QD in its GS coexisting with n cavity photons. The same for states Xn with the QD in its excited state X. Double continuous lines depict the coupling g, dashed lines the pumping with rate P, dotted lines the leaky modes emission with rate γ, and dash-dotted lines the emission of cavity modes with rate κ.

Eq. (7) one can get a set of differential equations that describe the evolution of the populations and coherences of the cavity-QD system. On the basis $(|Gn\rangle;|Xn\rangle)$ of product states between QD states and Fock states of the cavity mode, the matrix elements of the reduced density matrix are

$$\rho_{in,jm}=\langle in|\rho|jm\rangle, \tag{8}$$

with i, j being either G or X. The diagonal matrix elements $\rho_{Gn,Gn}$, $\rho_{Xn,Xn}$ are the populations of the QD-photon levels, while the nondiagonal terms $\rho_{Gn,Xn-1}$, $\rho_{Xn-1,Gn}$, describe the coherences between these levels. By taking the matrix elements in Eq. (7) we get, for $t=0$, the following set of linear differential equations:

$$\begin{aligned}\partial_t\rho_{Gn,Gn}=&\, ig\sqrt{n}(\rho_{Gn,Xn-1}-\rho_{Xn-1,Gn})+\gamma\rho_{Xn,Xn}\\&-\kappa[n\rho_{Gn,Gn}-(n+1)\rho_{Gn+1,Gn+1}]-P\rho_{Gn,Gn},\end{aligned} \tag{9}$$

$$\begin{aligned}\partial_t\rho_{Xn,Xn}=&\, ig\sqrt{n+1}(\rho_{Xn,Gn+1}-\rho_{Gn+1,Xn})-\gamma\rho_{Xn,Xn}\\&-\kappa[n\rho_{Xn,Xn}-(n+1)\rho_{Xn+1,Xn+1}]+P\rho_{Gn,Gn},\end{aligned} \tag{10}$$

$$\begin{aligned}\partial_t\rho_{Gn,Xn-1}=&\, i[g\sqrt{n}(\rho_{Gn,Gn}-\rho_{Xn-1,Xn-1})+\Delta\rho_{Gn,Xn-1}]\\&-[(\gamma+\kappa(2n-1)+P)/2]\rho_{Gn,Xn-1}\\&+\kappa\sqrt{n(n+1)}\rho_{Gn+1,Xn},\end{aligned} \tag{11}$$

plus the equation Hermitian conjugate of (11). In the absence of dissipation, the matrix elements $\rho_{Gn,Gn}$, $\rho_{Xn-1,Xn-1}$, $\rho_{Gn,Xn-1}$, and $\rho_{Xn-1,Gn}$, for a given photon number n, satisfy a closed set of four differential equations. However, the pumping and emission with rates P, κ, and γ, couple the terms with different photon occupation number n, so that an infinite set of equations has to be solved, as depicted schematically in Fig. 1. For the numerical integration, the set of equations can be truncated at a given value that, in all the cases considered below, it is enough to take equal to 100.

As initial conditions we take $\rho_{G0,G0}=1$ and all the other elements of the density matrix equal to zero. In other words, we start with the system in its ground state and the pumping, and subsequently the losses, produces the dynamical evolution of the whole system. The steady state of the system can be studied by integrating the set of Eqs. (9)–(11) for long times.

C. First- and second-order coherence functions

From the master equation, one can compute the dynamics of the expectation values of any operator. Moreover, two-time correlation functions are also of physical interest. In particular, we want to compute the first- and second-order coherence functions[3,4]

$$g^{(1)}(\vec{r},t,\tau)=\frac{\langle E^{(-)}(\vec{r},t)E^{(+)}(\vec{r},t+\tau)\rangle}{\sqrt{\langle E^{(-)}(\vec{r},t)E^{(+)}(\vec{r},t)\rangle\langle E^{(-)}(\vec{r},t+\tau)E^{(+)}(\vec{r},t+\tau)\rangle}}, \tag{12}$$

$$g^{(2)}(\vec{r},t,\tau)=\frac{\langle E^{(-)}(\vec{r},t)E^{(-)}(\vec{r},t+\tau)E^{(+)}(\vec{r},t+\tau)E^{(+)}(\vec{r},t)\rangle}{\langle E^{(-)}(\vec{r},t)E^{(+)}(\vec{r},t)\rangle\langle E^{(-)}(\vec{r},t+\tau)E^{(+)}(\vec{r},t+\tau)\rangle}, \tag{13}$$

where $E^{(+)}$ and $E^{(-)}$ are the positive and negative frequency parts of the amplitude of the electromagnetic field. In the steady-state limit in which we are interested, neither $g^{(1)}$ nor $g^{(2)}$ depends on the absolute time t.

The experimental situation is such that photonic modes escaping from the cavity are emitted in well-defined directions, for instance along the axis of the micropillars in the direction in which the mirrors defining the cavity have some transparency.[5,6,8–11] On the contrary, emission of leaky modes takes place in any direction, particularly through lateral surfaces of the micropillar. This means that simply by changing the spatial distribution of detectors, one can measure the emission from cavity modes or the leaky modes.

By Fourier transforming the first-order correlation function

$$G^{(1)}(t,\tau)=\langle E^{(-)}(\vec{r},t)E^{(+)}(\vec{r},t+\tau)\rangle, \tag{14}$$

one can obtain the the power spectrum of the emitted light,

$$S(\vec{r},\nu)=\frac{1}{\pi}\Re\int_0^\infty d\tau e^{i\nu\tau}G^{(1)}(t,\tau). \tag{15}$$

The first-order correlation function of the external field can be obtained from the time dependence of the operators describing intrinsic properties of the system

$$\begin{aligned}G_C^{(1)}(t,\tau)&=\langle a^\dagger(t+\tau)a(t)\rangle,\\ G_X^{(1)}(t,\tau)&=\langle\sigma^\dagger(t+\tau)\sigma(t)\rangle.\end{aligned} \tag{16}$$

$G_C^{(1)}(t,\tau)$ is the correlation function for the cavity mode, responsible for the stimulated emission part of the spectrum (i.e., the light coming from the confined photon) by means of $G^{(1)}(t,\tau)\propto\kappa G_C^{(1)}(t,\tau)$. In the case of pillar microcavities, it

would correspond to the light emitted in the vertical direction. On the other hand $G_X^{(1)}(t,\tau)$ describes the spontaneous part of the spectrum (i.e., light directly coupled to the QD exciton) by means of $G^{(1)}(t,\tau) \propto \gamma G_X^{(1)}(t,\tau)$. This gives the light emitted through the leaky modes that can be measured in the lateral direction of a micropillar.

In order to calculate these two-time correlation functions, we make use of the quantum regression theorem.[2–4] First of all, we define the following operators:

$$a_{Gn}^{\dagger}(\tau) = |Gn+1\rangle\langle Gn| e^{i(\omega-\Delta)\tau},$$

$$a_{Xn}^{\dagger}(\tau) = |Xn+1\rangle\langle Xn| e^{i(\omega-\Delta)\tau},$$

$$\sigma_n^{\dagger}(\tau) = |Xn\rangle\langle Gn| e^{i\omega\tau},$$

$$\varsigma_n(\tau) = |Gn+1\rangle\langle Xn-1| e^{i(\omega-2\Delta)\tau}. \tag{17}$$

In the interaction picture, time evolution with respect to $H_{X-C}+H_{RS}$ appears explicitly. The two-time correlation function of the cavity mode can be expressed in terms of the previous operators:

$$G_C^{(1)}(t,\tau) = \sum_n \sqrt{n+1}[\langle a_{Gn}^{\dagger}(t+\tau)a(t)\rangle + \langle a_{Xn}^{\dagger}(t+\tau)a(t)\rangle]. \tag{18}$$

The exciton correlation function can be written as follows:

$$G_X^{(1)}(t,\tau) = \sum_n \langle \sigma_n^{\dagger}(t+\tau)\sigma(t)\rangle. \tag{19}$$

For the calculation of the spectrum of the emitted light it is, thus, necessary to evaluate the functions $\langle a_{Gn}^{\dagger}(t+\tau)a(t)\rangle$, $\langle a_{Xn}^{\dagger}(t+\tau)a(t)\rangle$, and $\langle \sigma_n^{\dagger}(t+\tau)\sigma(t)\rangle$. The quantum regression theorem states that given a set of operators O_j, whose averages satisfy a closed set of linear differential equations

$$\frac{d}{d\tau}\langle O_j(t+\tau)\rangle = \sum_k L_{j,k}\langle O_k(t+\tau)\rangle, \tag{20}$$

then the two-time averages of O_j with any other operator O, also satisfy the same differential equation

$$\frac{d}{d\tau}\langle O_j(t+\tau)O(t)\rangle = \sum_k L_{j,k}\langle O_k(t+\tau)O(t)\rangle. \tag{21}$$

In order to get the time evolution of two-time averages, we start with the dynamics of the operators in (17). Their averages satisfy the set of linear differential equations that allows us to find the evolution of the corresponding two-time averages in Eqs. (18) and (19),

$$\partial_\tau\langle a_{Gn}^{\dagger}(\tau)\rangle = (\partial_\tau\rho_{Gn,Gn+1})e^{i(\omega-\Delta)\tau} + i(\omega-\Delta)\langle a_{Gn}^{\dagger}(\tau)\rangle,$$

$$\partial_\tau\langle \sigma_n^{\dagger}(\tau)\rangle = (\partial_\tau\rho_{Gn,Xn})e^{i\omega\tau} + i\omega\langle \sigma_n^{\dagger}(\tau)\rangle,$$

$$\partial_\tau\langle a_{Xn-1}^{\dagger}(\tau)\rangle = (\partial_\tau\rho_{Xn-1,Xn})e^{i(\omega-\Delta)\tau} + i(\omega-\Delta)\langle a_{Xn-1}^{\dagger}(\tau)\rangle,$$

$$\partial_\tau\langle \varsigma_n(\tau)\rangle = (\partial_\tau\rho_{Xn-1,Gn+1})e^{i(\omega-2\Delta)\tau} + i(\omega-2\Delta)\langle \varsigma_n(\tau)\rangle. \tag{22}$$

Although the operator ς_n is not needed in the evaluation of the required two-time averages (18) and (19), we have to add the correlation functions that include an operator ς_n, in order to get a closed set of equations. Using the master equation and eliminating the elements of the density matrix, we arrive at the desired time evolution for the averages of the operators in Eqs. (17)

$$\begin{aligned}\partial_\tau\langle a_{Gn}^{\dagger}(\tau)\rangle = {}& \langle a_{Gn}^{\dagger}(\tau)\rangle\left[i(\omega_X-\Delta) - \frac{\kappa}{2}(2n+1) - P\right] \\ & + \langle a_{Gn+1}^{\dagger}(\tau)\rangle\kappa\sqrt{(n+1)(n+2)} + \langle \sigma_n^{\dagger}(\tau)\rangle ig\sqrt{n+1} \\ & + \langle a_{Xn-1}^{\dagger}(\tau)\rangle\gamma - \langle \varsigma_n(\tau)\rangle ig\sqrt{n},\end{aligned}$$

$$\begin{aligned}\partial_\tau\langle \sigma_n^{\dagger}(\tau)\rangle = {}& \langle a_{Gn}^{\dagger}(\tau)\rangle ig\sqrt{n+1} + \langle \sigma_n^{\dagger}(\tau)\rangle\left[i\omega_X - \frac{(\gamma+P)}{2} - \kappa n\right] \\ & + \langle \sigma_{n+1}^{\dagger}(\tau)\rangle\kappa(n+1) - \langle a_{Xn-1}^{\dagger}(\tau)\rangle ig\sqrt{n},\end{aligned}$$

$$\begin{aligned}\partial_\tau\langle a_{(Xn-1)}^{\dagger}(\tau)\rangle = {}& \langle a_{Gn}^{\dagger}(\tau)\rangle P - \langle \sigma_n^{\dagger}(\tau)\rangle ig\sqrt{n} \\ & + \langle a_{Xn-1}^{\dagger}(\tau)\rangle\left[i(\omega_X-\Delta) - \gamma - \frac{\kappa}{2}(2n-1)\right] \\ & + \langle a_{Xn}^{\dagger}(\tau)\rangle\kappa\sqrt{n(n+1)} + \langle \varsigma_n(\tau)\rangle ig\sqrt{n+1},\end{aligned}$$

$$\begin{aligned}\partial_\tau\langle \varsigma_n(\tau)\rangle = {}& -\langle a_{(Gn)}^{\dagger}(\tau)\rangle ig\sqrt{n} + \langle a_{(Xn-1)}^{\dagger}(\tau)\rangle ig\sqrt{n+1} + \langle \varsigma_n(\tau)\rangle \\ & \times\left[i(\omega_X-\Delta) - \frac{(\gamma+P)}{2} - \kappa n\right] \\ & + \langle \varsigma_{n+1}(\tau)\rangle\kappa\sqrt{n(n+2)}.\end{aligned} \tag{23}$$

From Eq. (23) and the quantum regression theorem, it is straightforward to obtain two separate closed sets of differential equations for two times functions; one for the set of functions

$$\begin{aligned}&\{\langle a_{Gn}^{\dagger}(\tau+t)a(t)\rangle, \langle a_{Xn-1}^{\dagger}(\tau+t)a(t)\rangle, \\ &\langle \sigma_n^{\dagger}(\tau+t)a(t)\rangle, \langle \varsigma_n(\tau+t)a(t)\rangle\},\end{aligned} \tag{24}$$

needed for the calculation of $G_C^{(1)}(t,\tau)$, and the other for the set of functions

$$\begin{aligned}&\{\langle a_{Gn}^{\dagger}(\tau+t)\sigma(t)\rangle, \langle a_{Xn-1}^{\dagger}(\tau+t)\sigma(t)\rangle, \\ &\langle \sigma_n^{\dagger}(\tau+t)\sigma(t)\rangle, \langle \varsigma_n(\tau+t)\sigma(t)\rangle\},\end{aligned} \tag{25}$$

needed for the calculation of $G_X^{(1)}(t,\tau)$.

An important point is the initial conditions to solve these systems of equations. Such conditions are obtained by solving, up to the stationary limit, the master equations (9)–(11) for the density matrix. From this information, one knows the initial conditions. For the functions in (24),

$$\langle a^{\dagger}_{Gn}(t)a(t)\rangle = \sqrt{n+1}\rho_{Gn+1,Gn+1},$$

$$\langle a^{\dagger}_{Xn-1}(t)a(t)\rangle = \sqrt{n}\rho_{Xn,Xn},$$

$$\sigma^{\dagger}_{n}(t)a(t) = \sqrt{n+1}\rho_{Gn+1,Xn}e^{-i\Delta t},$$

$$\langle \varsigma_n(t)a(t)\rangle = \sqrt{n}\rho_{Xn,Gn+1}e^{i\Delta t}. \quad (26)$$

For the functions in (25),

$$\langle a^{\dagger}_{Gn}(t)\sigma(t)\rangle = \rho_{Xn,Gn+1}e^{-i\Delta t},$$

$$\langle a^{\dagger}_{Xn-1}(t)\sigma(t)\rangle = 0,$$

$$\langle \sigma^{\dagger}_{n}\sigma(t)\rangle = \rho_{Xn,Xn},$$

$$\langle \varsigma_n\sigma(t)\rangle = 0. \quad (27)$$

The second-order coherence function is, *a priori*, more complicated to calculate. Averages of products of four operators at two different times have to be performed. This task becomes much simpler for the case of zero time delay. $g^{(2)}(t,\tau=0)$ is a one-time operator, which simplifies the calculation. In spite of loosing information, $g^{(2)}(t,\tau=0)$ is a very interesting magnitude because it can be used as an indicator of the possible coherence of the state of the system.[1–4] In addition, if we concentrate in the properties of cavity modes (i.e., neglecting the emission of leaky modes), the second-order coherence function acquires a very simple form in the stationary limit

$$g^{(2)}(t,\tau=0) = \frac{\langle a^{\dagger}a^{\dagger}aa\rangle}{\langle a^{\dagger}a\rangle^2} = \frac{\sum_n n(n-1)[\rho_{Xn,Xn}+\rho_{Gn,Gn}]}{\left[\sum_n n[\rho_{Xn,Xn}+\rho_{Gn,Gn}]\right]^2}. \quad (28)$$

$g^{(2)}$ takes different values depending on the statistics of the photon state: $g^{(2)}=2$ for chaotic states, $g^{(2)}=1$ for states having a Poisson distribution in n, and $g^{(2)}<1$ for nonclassical systems having a sub-Poisson distribution.[2–4]

III. RESULTS

A. Election of the range of parameters of interest

Since our model has several parameters, we need some simple pictures in order to gain insight on the interesting regime of parameters. Although our system is similar to a spin-coupled to an harmonic oscillator, we can understand the effect of dissipation by considering two-coupled (by g) oscillators. One of them has an eigenfrequency $\omega_X-\Delta$ being damped with a rate κ while the other, with an eigenfrequency ω_X, is damped with a rate γ and is pumped incoherently with a rate P. The incoherent pumping implies a dephasing mechanism that, together with the damping, gives an average dephasing $(\gamma+P)/2$. When the damping of the first oscillator κ is much higher than the dephasing $(\gamma+P)/2$ of the second oscillator, one could expect that the frequency of this second oscillator ω_X will survive longer than $\omega_X-\Delta$, and it will dominate the spectrum. In the opposite limit, $\kappa \ll (\gamma+P)/2$, the frequency $\omega_X-\Delta$ will dominate the spectrum. This behavior is the one shown by our spin-oscillator system as can be checked by means of the Haken's model on adiabatic elimination[2,3,16] in the equations of motion of the field operators. From this simple picture, we can motivate the existence of three different regimes $\kappa \gg (\gamma+P)/2$, $\kappa \ll (\gamma+P)/2$, and some intermediate regimes. For this purpose, we fix $g=1$ as the energy scale, take a fixed small value $\gamma=0.1$ reflecting the fact that leaky modes emission is the less efficient mechanism in practical situations, and define the three regimes by changing κ and P.

Apart from those parameters, our model requires us to set the frequency of the two oscillators. In practical cases, the coupling between the oscillators is in the order of meV while the excitation energy ω_X is in the order of eV. Therefore, since our energy scale is $g=1$(meV), all the calculations we present here have been performed by taking $\omega_X=1000$. Finally the detuning Δ is a very important parameter. Since typical detunings are on the order of a few meV, we present here results for two different cases: perfect resonance $\Delta=0$ and quasiresonance $\Delta=5$.

B. Dynamics of the density matrix: Occupations and coherences

In this section we show the time evolution of the occupations and coherences (diagonal and off-diagonal, respectively) $\rho_{in,jm}$ described in Eqs. (9)–(11). From these equations, it is clear that if losses and pumping are not included, the system shows the usual Rabi oscillations in each subspace with a given number of photons. The amplitude of these oscillations increases with the coupling g and decreases with the detuning Δ.

When all the losses and the pumping are included, the situation changes drastically. The initial occupation of $|G0\rangle$ evolves with time up to a state of equilibrium in which occupation is redistributed among a large number of levels with a finite number of photons. In this final steady situation, the sum of all the losses equilibrates the pumping.

Figures 2 and 3 show the time evolution of occupations $\rho_{in,in}$ for both the exciton $(i\equiv X)$ and the ground $(i\equiv G)$ states in two cases with finite detuning Δ. The results in Figs. 2 and 3 are typical of the two regimes described above. The first point to be noted is the time scale of the transient regime, something that could be accessible by ultrafast spectroscopy. In the case in which pumping dominates (Fig. 2), the transient regime is of the order of 100 ps, while when the pumping is comparable with the emission rate (Fig. 3), such scale is reduced to just a few picoseconds. The second interesting point is the relative occupation of different states. When pumping rate P dominates (Fig. 2), states with a large number of photons n become occupied and two bundles of branches can be distinguished: upper branches corresponding to $|Xn\rangle$ states and lower branches corresponding to $|Gn\rangle$ states. In other words, the system stores many photons in the cavity preferably keeping the QD in its exciton state. When rates for photon emission increase and become comparable

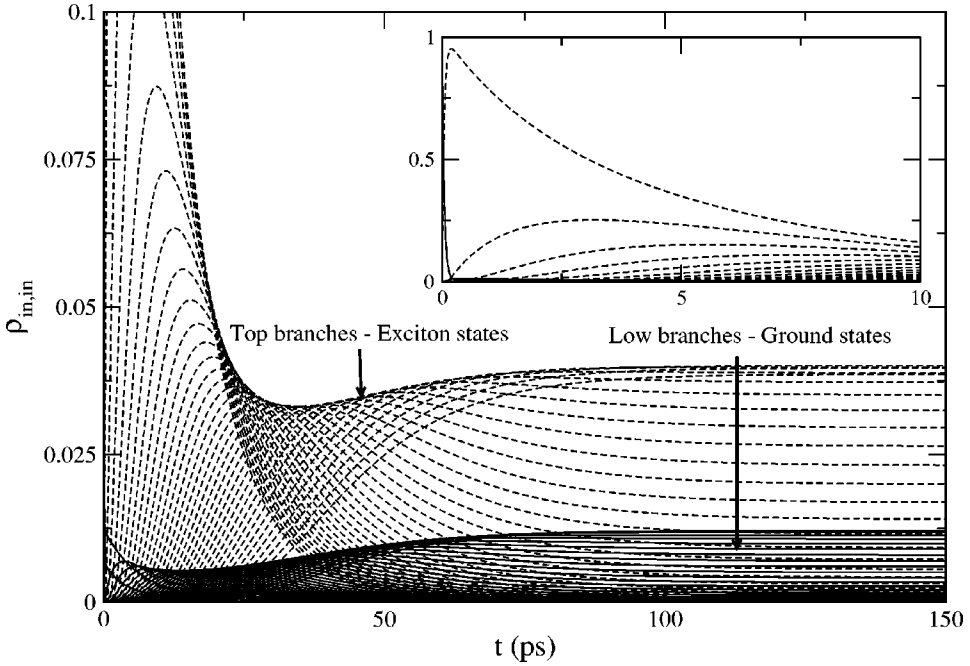

FIG. 2. Density matrix diagonal elements $\rho_{in,in}$ for exciton ($i \equiv X$) states (dashed lines), and ground ($i \equiv G$) states (continuous lines), from $n=0$ up to $n=35$ cavity photons. $g=1$, $\Delta=5$, $\gamma=0.1$, $\kappa=0.1$, and $P=15$. The inset shows a zoom out of the graphic to observe high occupations at very short times.

to the pumping rate, just a few photons ($n<3$) can be stored in the cavity but still, in the stationary situation, the highest occupation is that of the excitonlike state $|X0\rangle$. It is quite evident that an interesting regime is missing in these results: the one in which losses dominate onto the pumping, for instance the case $\kappa=5$ and $P=1$. We will discuss below other characteristics of this case, but do not include any figure here because the corresponding time dependence is featureless, showing a fast decay to zero of the occupations for all the states with $n>0$.

Time evolution of coherences $\rho_{X0,G1}$ is shown in Fig. 4 for the two limiting cases $P \gg \kappa$ and $P \ll \kappa$ for $\Delta=5$. These coherences present oscillations that are due to this finite detuning as we discuss below. When κ dominates, the coherences increase with time up to finite, but small, value. When pumping dominates, the mean number of photons inside the cavity is much higher than 1 as discussed below. Therefore, a coherence like the one in Fig. 4 between states with $n=0$ and $n=1$ decreases with time. In this case, $P \gg \kappa$, we have computed coherences $\rho_{Xn,Gn+1}$, for values of n around the mean number of photons inside the cavity (see below), obtaining that they also go to a small constant (apart from oscillations) for large times.

The oscillatory behavior of the coherences is produced by the second term at the right-hand side of Eq. (11). The detuning provokes a period $2\pi\hbar/\Delta$. In order to analyze the

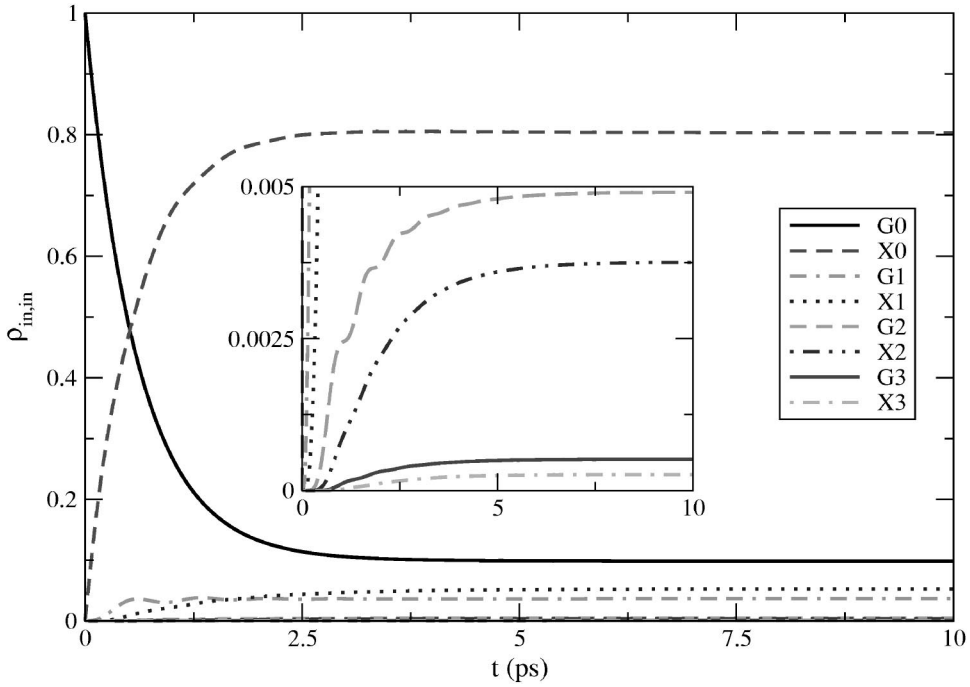

FIG. 3. Density matrix diagonal elements $\rho_{in,in}$ for both the exciton ($i \equiv X$) and the ground ($i \equiv G$) states, from $n=0$ up to $n=3$ cavity photons. $g=1$, $\Delta=5$, $\gamma=0.1$, $\kappa=0.5$, and $P=1$. The inset shows a zoom of the vertical axis of the graphic.

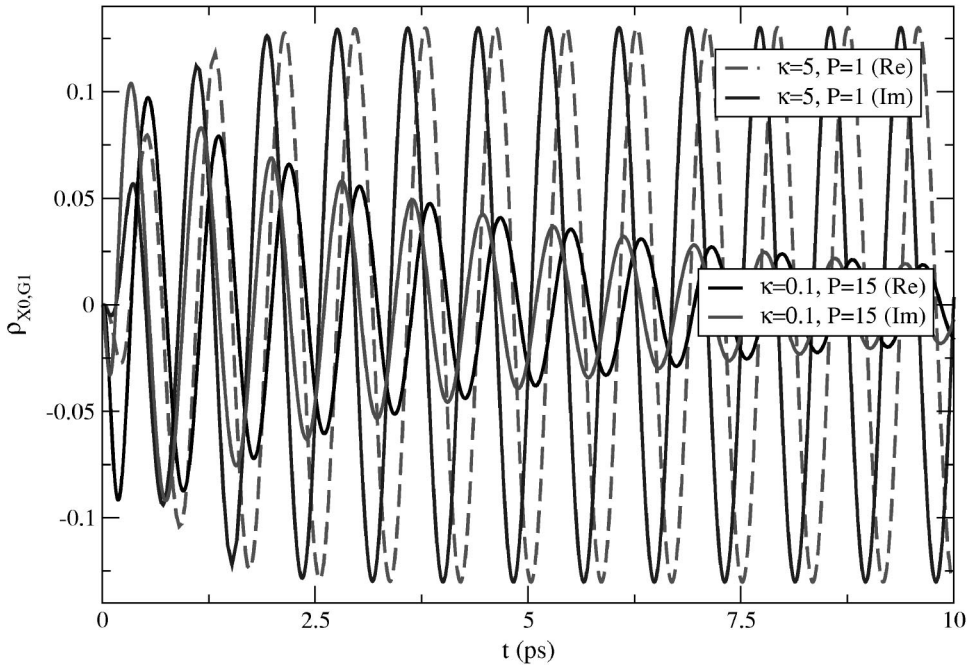

FIG. 4. Density matrix off diagonal element $\rho_{X0,G1}$ with detunning $\Delta=5$ for $g=1$, $\gamma=0.1$, and two different values of κ and P.

limiting case of perfect resonance, we show in Fig. 5 the coherences $\rho_{X0,G1}$ for some cases with $\Delta=0$. No oscillations exist in these cases. Moreover, all these off-diagonal elements of the density matrix become real while they were complex for finite detuning as shown in Fig. 4.

The fact, shown above, that P competes with κ, is not completely general. This fact can be seen in Eqs. (9)–(11) for the time evolution of the density matrix elements. For the off-diagonal terms, P has the same sign than the losses κ and γ, while for the diagonal terms, these signs are different. The pumping produces decoherence in the off-diagonal terms as the emission of photons does because in our model the pumping is incoherent. At the same time, P favors higher occupations (increase of the diagonal elements). Therefore it is clear that, for a high pumping, decays of the off-diagonal terms (loss of coherence) prevail on the occupation until the coherence is completely quenched and later inverted, preventing the evolution toward the occupation of states with a high number of photons. This is an indication of the important role that off-diagonal elements play in the time evolution. It also explains that, if the emission rate κ is above a critical value, it dominates on any pumping effect.

C. Number of cavity photons

A very important result to be drawn from the time evolution discussed above is the fact that the system is able to

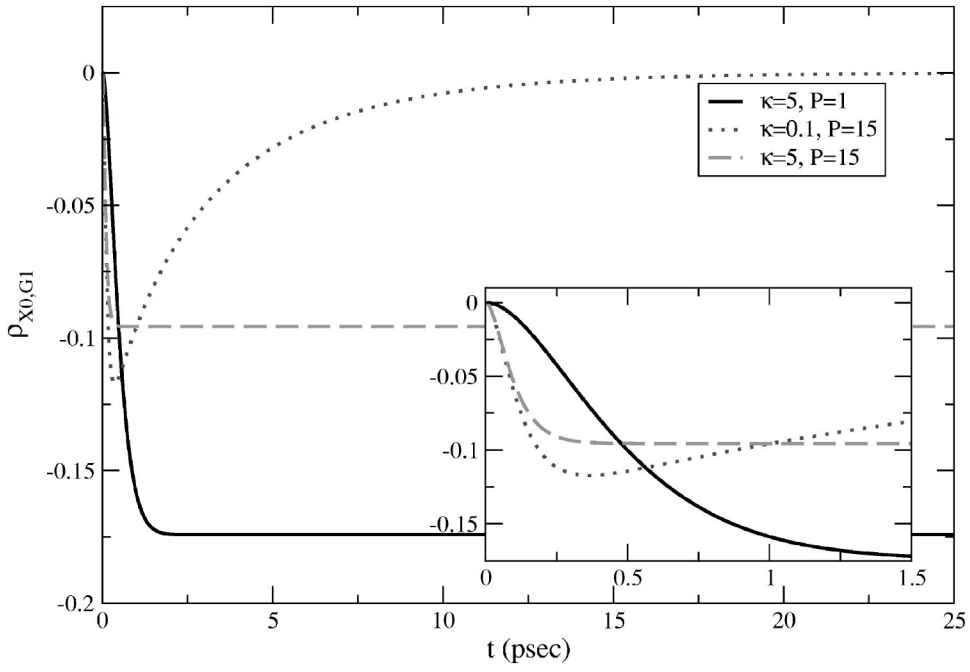

FIG. 5. Imaginary part of the density matrix off diagonal element $\rho_{X0,G1}$ at perfect resonance ($\Delta=0$) for $g=1$, $\gamma=0.1$, and different values of κ and P. All the real parts of the same matrix elements are zero. The inset shows a zoom of the graphic for small values of t.

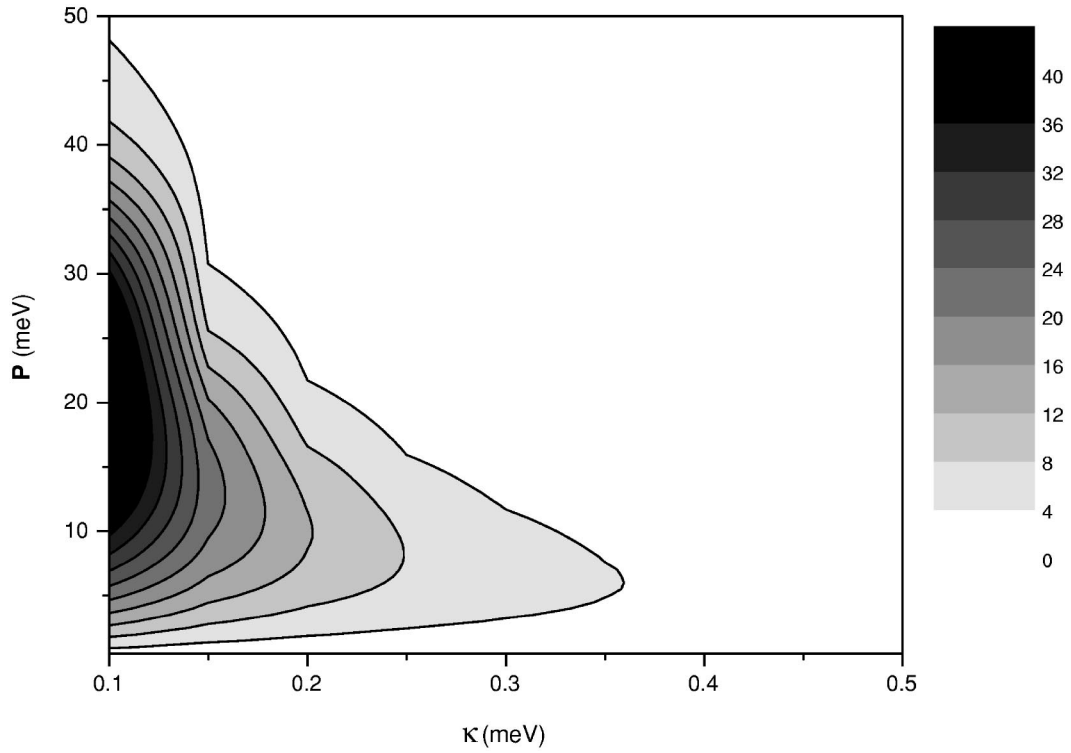

FIG. 6. $\overline{N_{ph}}$, in gray scale, as a function of κ and P for perfect resonance $\Delta=0$ with $g=1$ and $\gamma=0.1$. Some contours of constant $\overline{N_{ph}}$ are drawn as continuous lines to clarify the figure.

store a significant number of cavity photons. Let us analyze the mean number of cavity photons as a first step to study the quantum properties of these photons by looking to its distribution. The mean number of photons in the cavity is

$$\overline{N_{ph}} = \sum_n n(\rho_{Xn,Xn} + \rho_{Gn,Gn}). \tag{29}$$

$\overline{N_{ph}}$ increases with time, in a scale of hundreds of picoseconds, up to the stationary value that is the magnitude in which we are interested. Figures 6 and 7 show a contour plot of the mean number of cavity photons for $\Delta=0$ and $\Delta=5$, respectively. As in previous figures, we fix all the parameters except P and κ, which vary along the two axis. In these figures a region with a high $\overline{N_{ph}}$ can be observed. It corresponds to low emission and high pumping. The region is larger and the number of cavity photons higher, for the resonant case $\Delta=0$, than for the case with detuning $\Delta=5$. A detuning makes more difficult the coupling between the states $|Xn\rangle$ and $|Gn+1\rangle$. As a consequence the mechanism of storing cavity photons become less efficient.

A conclusion similar to the one drawn in the previous section is in order. When pumping increases, the mean number of cavity modes also increases up to a certain maximum value. Further increase of P implies that the dephasing mechanism related with this incoherent pumping provokes a decrease of $\overline{N_{ph}}$. Similar behavior was already described in Refs. 15 and 17 for the case of perfect resonance between the QD exciton and the cavity photon ($\Delta=0$). The comparison of Figs. 6 and 7 shows how a finite detuning noticeably reduces the range of pumping in which a large number of photons is stored in the cavity.

D. Second-order coherence function

The possibility of storing a large number of cavity photons for a wide range of parameters opens an interesting alternative beyond the simple value of $\overline{N_{ph}}$: how is the distribution of cavity photons? If any interesting distribution is involved, its character could be transfered to the light emitted by the system.

In order to quantify if such distributions are closer to Gaussian distributions (thermal or chaotic states), Poisson distributions, or even nonclassical sub-Poissonian distributions, one can compute, using Eq. (28), the second-order coherence function $g^{(2)}(\tau=0)$ discussed above. $g^{(2)}$ was also studied in Ref. 15 in the case of alternating pumping of electrons and holes. The modulation period strongly affects to the behavior of the second-order coherence function (see Fig. 8 of Ref. 15). Therefore, as we have done for all the others magnitudes, we present results obtained with continuous pumping.

Figures 8 and 9 show $g^{(2)}(0)$, for $\Delta=0$ and $\Delta=5$, respectively. In these two figures we have dashed the region in which $g^{(2)}(0)$ is close to 1 to show the region supporting a Poissonian distribution. This is the border between classically accessible region and the one having $g^{(2)}(0)<1$ with nonclassical states with sub-Poissonian distribution. In the case of perfect resonance (Fig. 8), for low κ, the Poissonian distribution region is rather wide in terms of the pumping P. When κ increases, this region becomes much narrower in P.

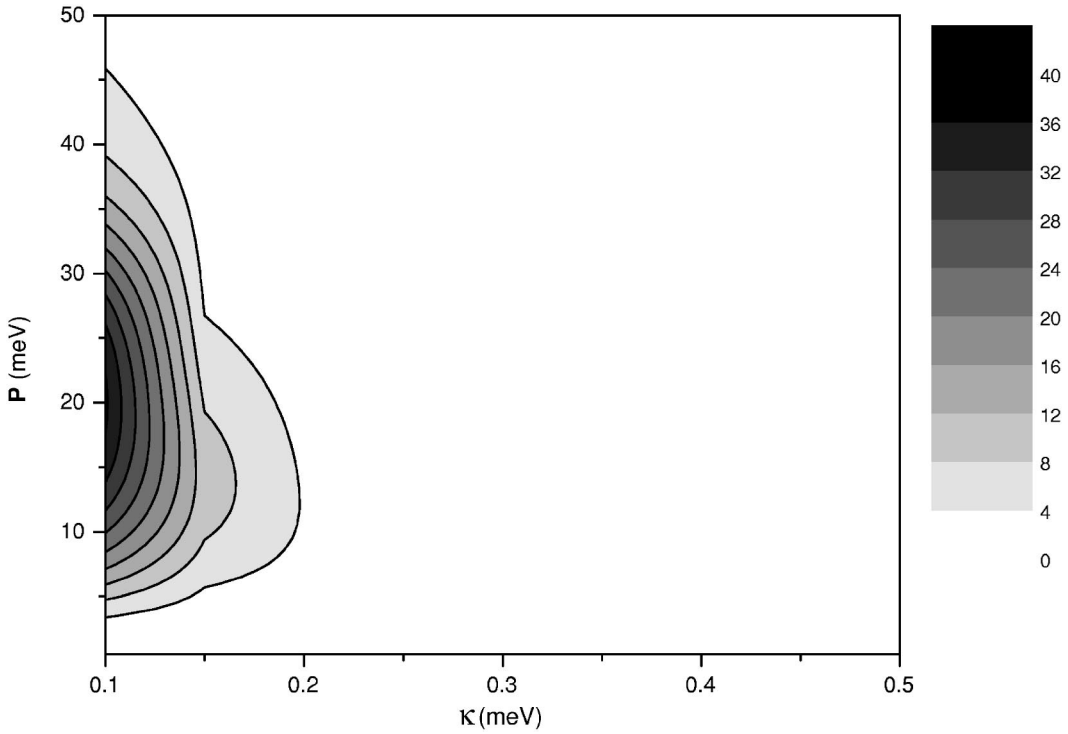

FIG. 7. $\overline{N_{ph}}$, in gray scale, as a function of κ and P for a detuning $\Delta=5$ with $g=1$ and $\gamma=0.1$. Some contours of constant $\overline{N_{ph}}$ are drawn as continuous lines to clarify the figure.

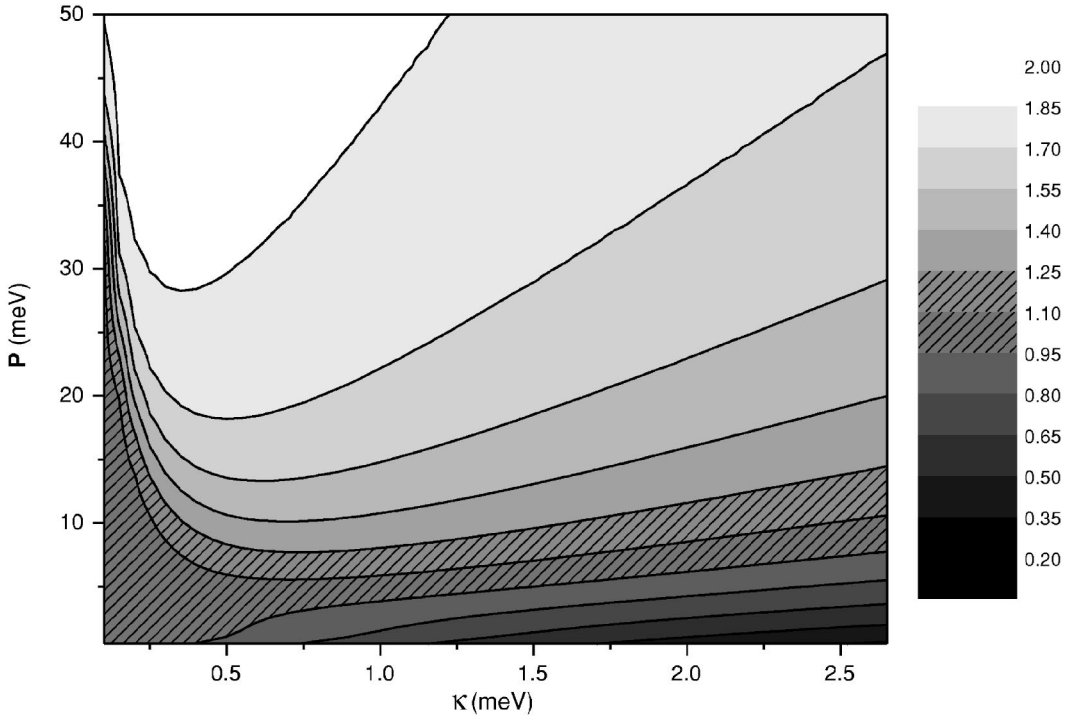

FIG. 8. Second-order coherence function $g^{(2)}(\tau=0)$, in gray scale, as function of κ and P for perfect resonance $\Delta=0$. $g=1$ and $\gamma=0.1$. The dashed area shows the region supporting a Poisson distribution of cavity photons in which $g^{(2)}(\tau=0)$ close to 1. Some contours of constant $g^{(2)}$ are drawn as continuous lines to clarify the figure.

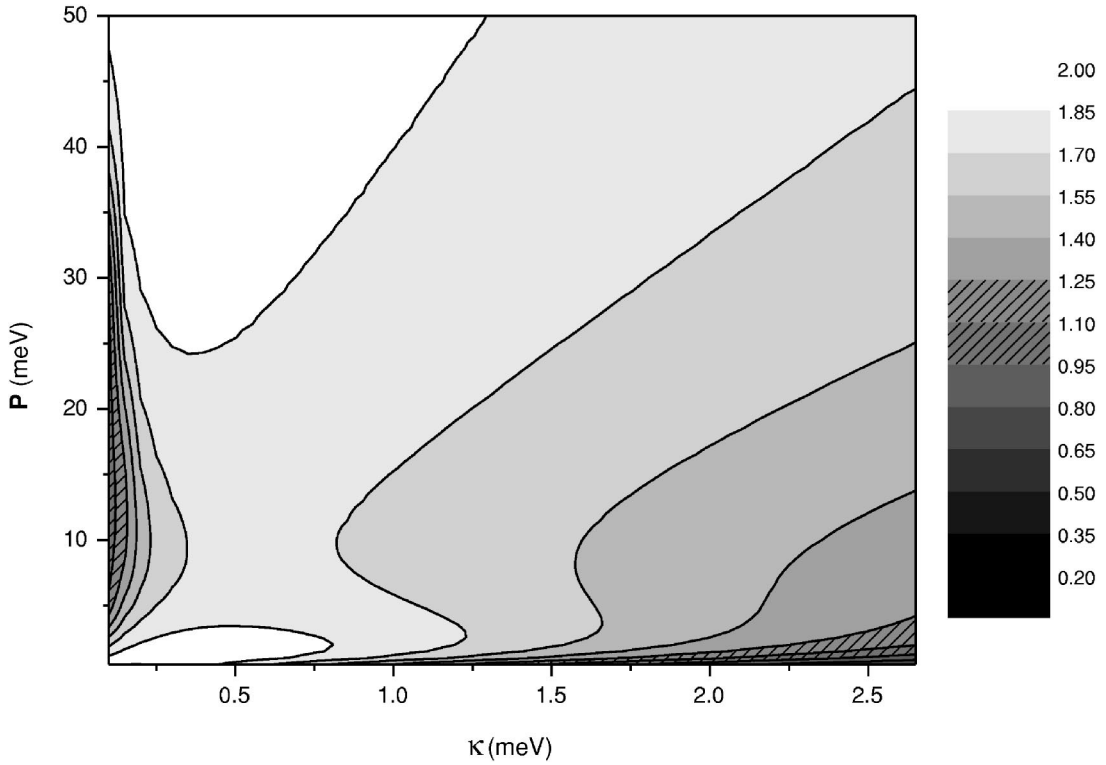

FIG. 9. Second-order coherence function $g^{(2)}(\tau=0)$, in gray scale, as function of κ and P for a detuning $\Delta=5$. $g=1$ and $\gamma=0.1$. The dashed area shows the region supporting a Poisson distribution of cavity photons in which $g^{(2)}(\tau=0)$ close to 1. Some contours of constant $g^{(2)}$ are drawn as continuous lines to clarify the figure.

In the case of detuning $\Delta=5$, the Poissonian region becomes much smaller and even disappearing for intermediate values of κ.

The interesting region of $g^{(2)}(0)<1$ appears for very low pumping in these two figures. Even though this occurs in a small region of parameters, it is very interesting because it means that the system can form squeezed photon states with sub-Poissonian distribution. In this region the emitted light shows the antibunching that is characteristic of nonclassical light emitters.

The rest of the diagram is supporting states with $g^{(2)}(0)$ increasing from 1 to 2, i.e., states where second-order coherence is reduced and approaching a Gaussian distribution $[g^{(2)}(0)=2]$. A finite detuning Δ enlarges this Gaussian region as observed when comparing the two figures.

Combining and summarizing the results of Figs. 6–9, it must be stressed that, for high-quality cavities, i.e., low γ and κ, and intermediate value of the incoherent pumping P is able to produce a rather large number of cavity photons with Poisson distribution. When detuning increases, this effect remains, although with a reduction of the region of parameters supporting it.

IV. SPECTRUM OF THE EMITTED LIGHT

In this section we will present our results for the spectrum of the emitted light in the stationary limit $(t\to\infty)$. This is the property that can be most easily measured in experiments. We will do it only in the case of finite detuning $\Delta=5$ in order to observe the emission at two different frequencies. Following the steps discussed in the section devoted to our model, we have computed $G_X^{(1)}(\tau)$ and $G_C^{(1)}(\tau)$ in the stationary limit $(t\to\infty)$ for the three regimes already discussed $P\gg\kappa$, $P\ll\kappa$, and P comparable to κ. Our results show fast oscillations modulated by an envelope that decreases to zero in a range of 10 ps for the case in which pumping dominates $(P\gg\kappa)$, while for the other two cases ($P\ll\kappa$ and P comparable to κ), the decay range reduces to 1 ps. In a second step, we Fourier transform these first-order correlation functions to calculate the spectrum of the emitted light. In order to numerically perform such Fourier-transforms, we have used digital data filters (Parzen and Haning) to reduce numerical noise. The spectra corresponding to $\omega_X=1000$ are shown in Figs. 10–12. In these three figures we have made use of the fact, discussed in the introduction, that the two types of emissions can be separated: the emission coming from the cavity modes takes place along the axis of the pillars, while the emission of leaky modes takes place in any spatial direction (mainly in the directions perpendicular to the axis of the pillar).

The case of Fig. 10 corresponds to a high pumping dominating on the effect of κ. As discussed above, one expects a strong damping of the oscillator with frequency ω_X. Therefore, only one peak at $\omega_X-\Delta$ is observed. Moreover, the peak shown in this spectrum is significantly narrower than the features observed in any other case we have analyzed as, for instance, the ones in the following figures.

Figure 11 shows the result with a high value of the rate emission $\kappa=5$ and a smaller, although nonnegligible, pump-

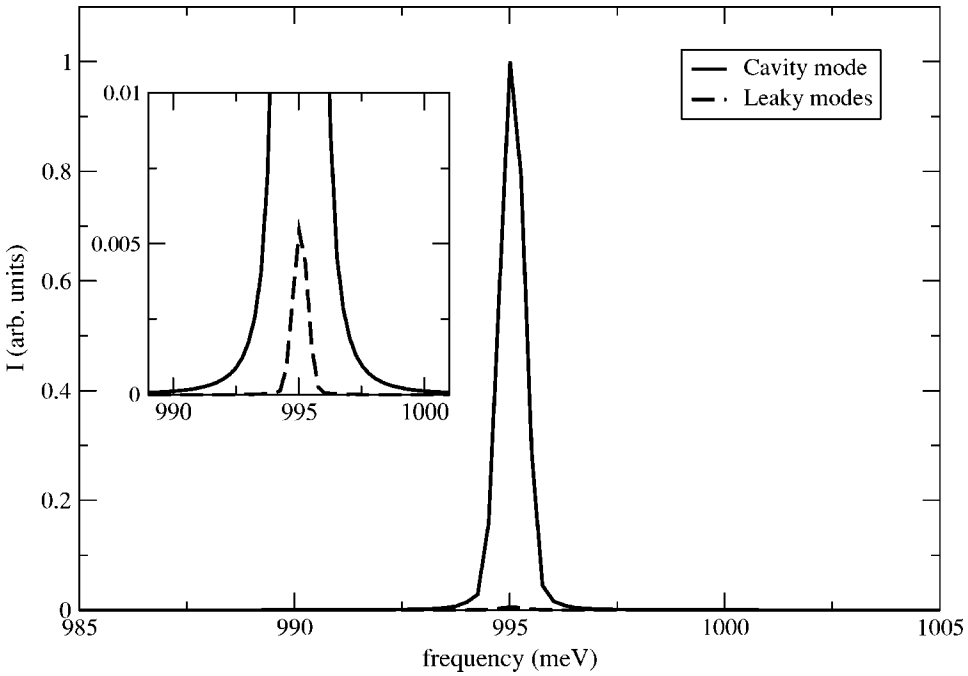

FIG. 10. Spectrum of emission for $g=1$, $\omega_X=1000$, $\Delta=5$, $\gamma=0.1$, $\kappa=0.1$, and $P=15$.

ing $P=1$. This case corresponds to $\overline{N_{ph}}=0.027$ and $g^{(2)}(0)=0.396$, i.e., to a sub-Poissonian distribution of a small number of cavity photons. Now, the strong damping of the mode with frequency $\omega_X-\Delta$ reduces its intensity, which becomes smaller than a second peak at ω_X.

In the intermediate case shown in Fig. 12, the dephasing of the two modes is similar and this produces a very wide peak at the spectrum as observed in the figure.

Let us finally analyze more carefully the case of the high-quality cavity (already studied in Fig. 10). For this purpose, we maintain fixed a low value $\kappa=0.1$ and let the pumping vary in a wide range of values. Figures 13 and 14 show the spectra of the stimulated (cavity) and spontaneous (leaky) emissions, respectively. First of all one must observe that scale in Fig. 13 is more than 200 times larger than that of Fig. 14, as it could be expected from the results and discussion of Fig. 10. The main result to be drawn from Figs. 13 and 14 is that the most intense emission corresponds to the range $10 \leqslant P \leqslant 30$ simply because this is the range of higher number of photons inside the cavity as shown in Fig. 7.

V. SUMMARY

We have described the dynamics of a QD embedded in a semiconductor microcavity by means of a two-level system strongly coupled to a single-cavity mode. The system is con-

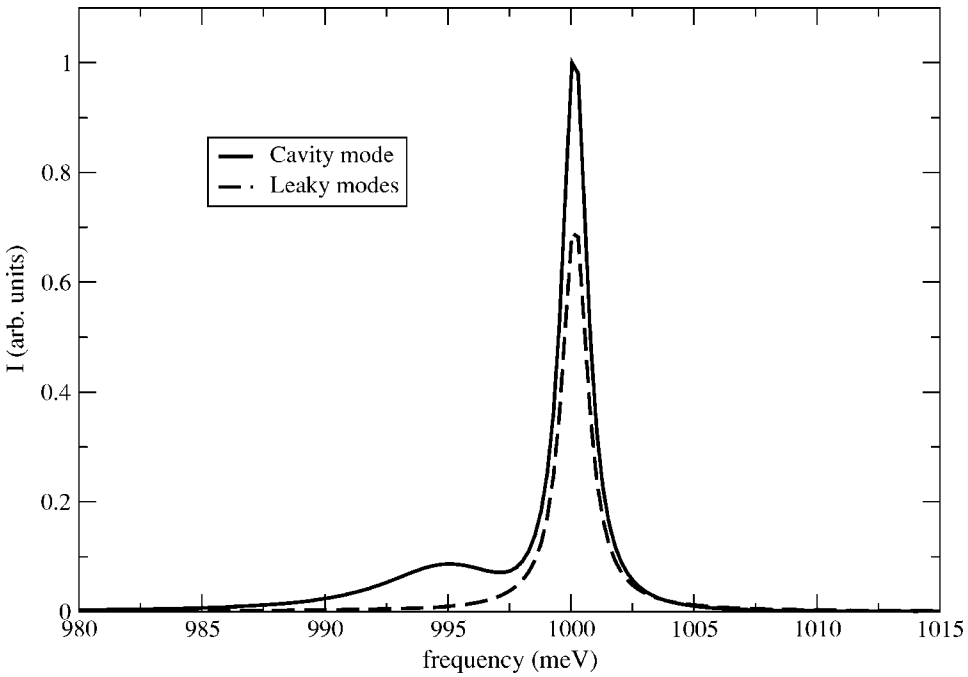

FIG. 11. Spectrum of emission for $g=1$, $\omega_X=1000$, $\Delta=5$, $\gamma=0.1$, $\kappa=5$, and $P=1$.

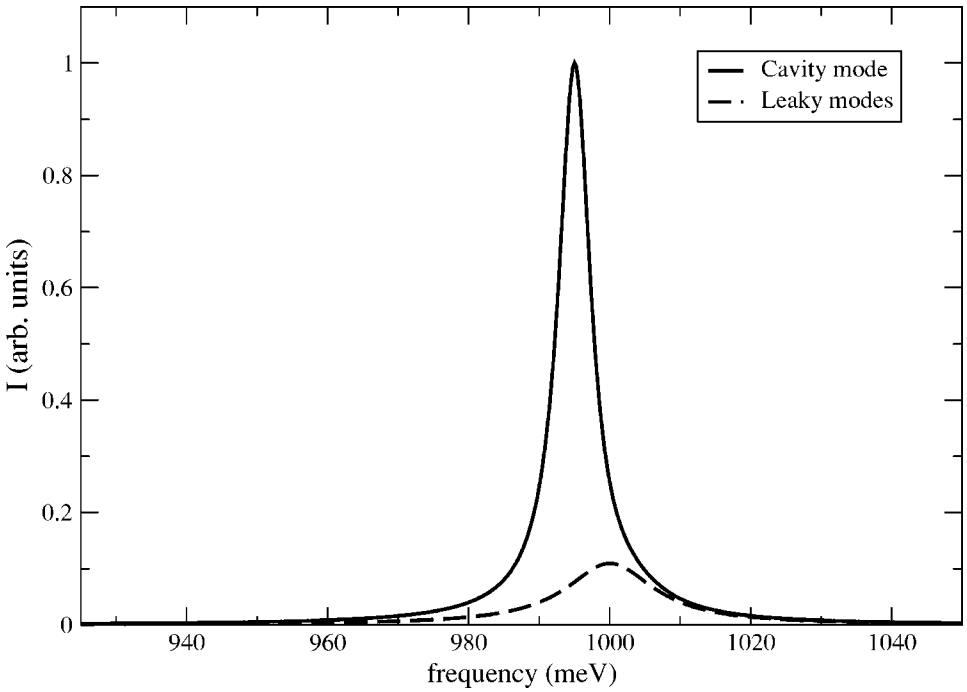

FIG. 12. Spectrum of emission for $g=1$, $\omega_X=1000$, $\Delta=5$, $\gamma=0.1$, $\kappa=5$, and $P=15$.

tinuously excited by incoherent pumping of excitons. Two different sources of photon emission are considered: spontaneous emission through a leaky mode and stimulated emission of a cavity mode escaping from the cavity. The time evolution of first- and second-order coherence functions is calculated. When pumping dominates over emission rates, a large number of cavity photons can be stored in the cavity. Further increase of the pumping introduces dephasing and a decrease of the number of cavity photons. These different regimes are also characterized by Poissonian or Gaussian photon distributions inside the cavity. Sub-Poissonian distributions can be obtained for a range of parameters, in which the pumping rate is very small, and the quantum nature of the QD-cavity system manifests itself in the emitted light. Finally, we have studied the emission spectrum of our system. In the case of high pumping dominating on the rate emission κ, one gets a strong damping of the oscillator corresponding to the exciton level with frequency ω_X, and only

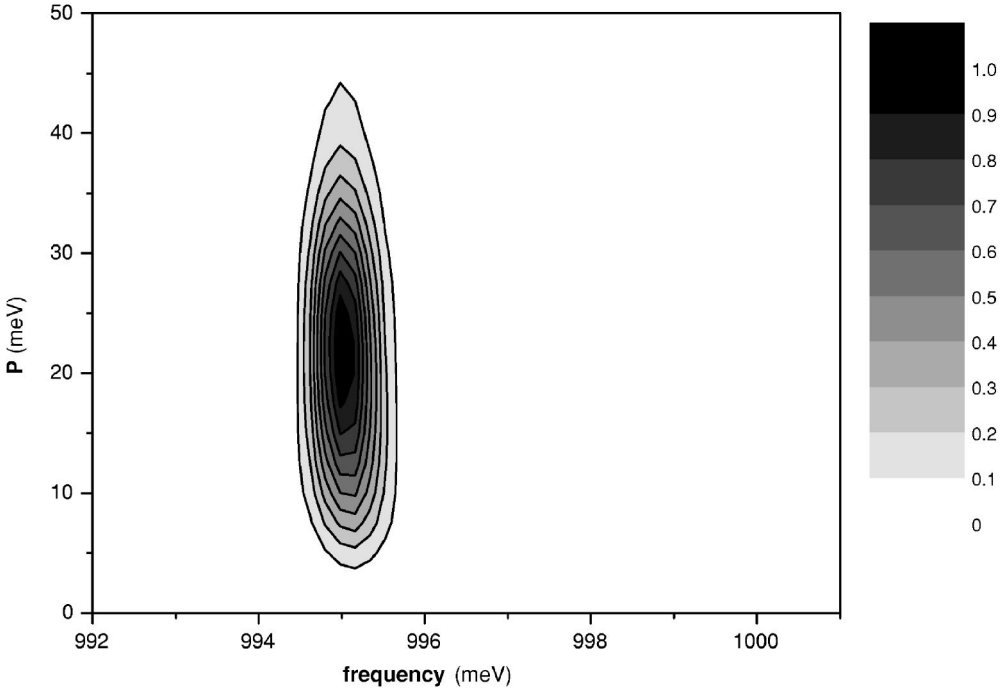

FIG. 13. Spectrum, in gray scale, of stimulated emission (cavity modes escaping from the cavity) as a function of frequency and P. $g=1$, $\omega_X=1000$, $\Delta=5$, $\gamma=0.1$, and $\kappa=0.1$. Some contours of constant intensity are drawn as continuous lines to clarify the figure.

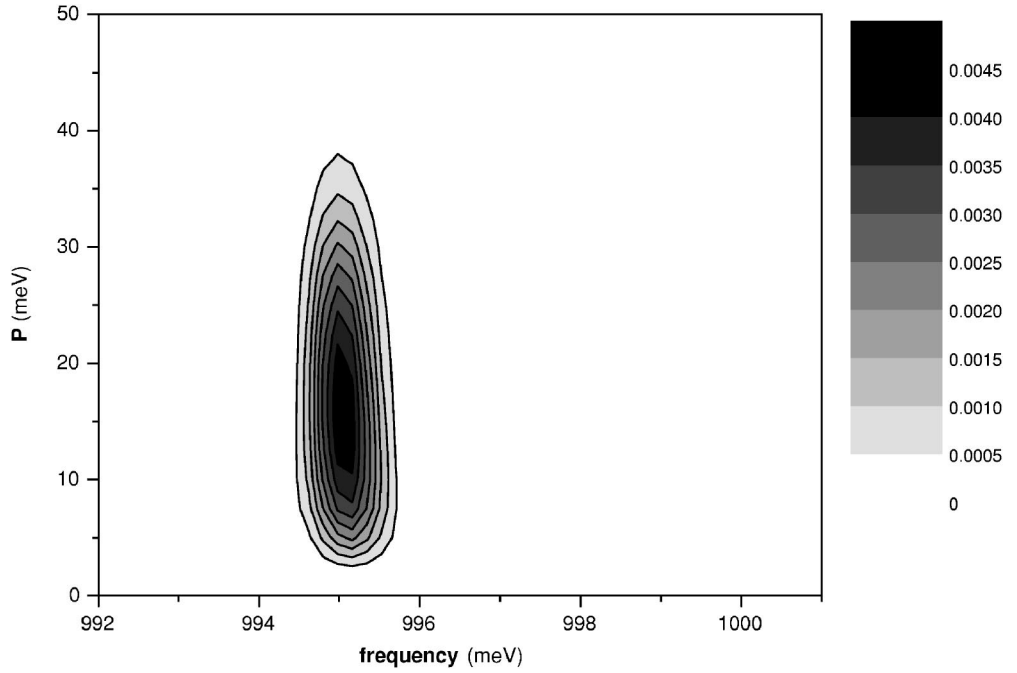

FIG. 14. Spectrum, in gray scale, of spontaneous emission (emission of leaky modes) as a function of frequency and P. $g=1$, $\omega_X=1000$, $\Delta=5$, $\gamma=0.1$, and $\kappa=0.1$. Some contours of constant intensity are drawn as continuous lines to clarify the figure.

one very narrow peak at $\omega_X-\Delta$ is observed. When the rate emission κ is higher than a nonnegligible pumping rate P, the strong damping of the mode with frequency $\omega_X-\Delta$ allows one to observe the two modes with a higher intensity for the mode at ω_X. In an intermediate case, the dephasing of the two modes is similar producing a very wide peak at the spectrum.

ACKNOWLEDGMENTS

We are indebted to Dr. P. Hawrylak for helpful discussions within the framework of the CERION2 project. Work supported in part by MCYT of Spain under Contract No. MAT2002-00139 and CAM under Contract No. 07N/0042/2002. The numerical work has been carried out in part at the CCC of UAM within the project QUANTUMDOT.

*Present address: Max-Planck Institute for Quantum Optics, D-85748 Garching, Germany.

[1] C. Cohen-Tannoudji, J. Dupont-Roc, and G. Grynberg, *Atom-photon Interactions* (Wiley-Interscience, New York, 1992).
[2] D. F. Walls and G. J. Milburn, *Quantum Optics* (Springer-Verlag, Berlin, 1994).
[3] M. O. Scully and M. S. Zubairy, *Quantum Optics* (Cambridge University Press, Cambridge, England, 1997).
[4] Y. Yamamoto and A. Imamoglu, *Mesoscopic Quantum Optics* (Wiley, New York, 1999).
[5] J. M. Gerard, B. Sermage, B. Gayral, B. Legrand, E. Costard, and V. Thierry-Mieg, Phys. Rev. Lett. **81**, 1110 (1998).
[6] O. Benson, C. Santori, M. Pelton, and Y. Yamamoto, Phys. Rev. Lett. **84**, 2513 (2000).
[7] P. Michler, A. Kiraz, C. Becher, W. V. Schoenfeld, P. M. Petroff, L. Zhang, E. Hu, and A. Imamoglu, Science **290**, 2282 (2000).
[8] G. S. Solomon, M. Pelton, and Y. Yamamoto, Phys. Rev. Lett. **86**, 3903 (2001).
[9] E. Moreau, I. Robert, J. M. Gerard, I. Abram, L. Manin, and V. Thierry-Mieg, Appl. Phys. Lett. **79**, 2865 (2001).
[10] C. Santori, D. Fattal, J. Vuckovic, G. S. Solomon, and Y. Yamamoto, Nature (London) **419**, 594 (2002).
[11] M. Pelton, C. Santori, J. Vuckovic, B. Zhang, G. Solomon, J. Plant, and Y. Yamamoto, Phys. Rev. Lett. **89**, 233602 (2002).
[12] T. M. Stace, G. J. Milburn, and C. H. W. Barnes, Phys. Rev. B **67**, 085317 (2003).
[13] Y. Yamamoto, M. Pelton, C. Santori, G. S. Solomon, O. Benson, J. Vuckovic, and A. Scerer, in *Semiconductor Spintronics and Quantum Computation*, edited by D. D. Awschalom, D. Loss, and N. Samarth (Springer-Verlag, New York, 2002), and references therein.
[14] A. V. Kozlovskii and A. N. Oraevskii, JETP **88**, 666 (1999).
[15] O. Benson and Y. Yamamoto, Phys. Rev. A **59**, 4756 (1999).
[16] G. W. Gardiner, *Handbook of Stochastic Methods* (Springer-Verlag, Berlin, 1983).
[17] Y. Mu and C. M. Savage, Phys. Rev. A **46**, 5944 (1992).